ELSEVIER

Chemical Engineering Journal 75 (1999) 167–176

Chemical Engineering Journal

www.elsevier.com/locate/cej

Perturbation method in gas-assisted power-law fluid displacement in a circular tube and a rectangular channel

Fethi Kamişli[*,1], Michael E. Ryan

Department of Chemical Engineering, State University of New York at Buffalo, Amherst, NY 14260, USA

Received 10 June 1998; received in revised form 25 May 1999; accepted 7 June 1999

Abstract

In this paper the two dimensional flow of a power-law fluid is studied analytically using a singular perturbation method in order to determine the residual liquid film thickness of power-law fluids on the wall of a circular tube or a rectangular channel when displaced by another immiscible fluid. Inner and outer expansions are developed in terms of a small parameter $C_A^{1/3}$ (modified capillary number). A differential equation for the shape of gas bubble is solved numerically in order to determine the inner solution. The method of matched asymptotic expansions is used to match the inner and outer solutions. This approach indicated that the residual liquid film thickness of non-Newtonian fluids increases with decreasing power-law index. © 1999 Elsevier Science S.A. All rights reserved.

Keywords: Two-phase flow; Perturbation method; Gas-assisted flow

1. Introduction

The motion of long bubbles into Newtonian fluids confined in horizontal cylindrical tubes or channels of rectangular cross-section (Hele–Shaw cell) has been studied for many years. When a less viscous fluid displaces a more viscous fluid from the gap between two closely spaced parallel plates, the interface develops a tongue-like shape with the less viscous fluid penetrating into the more viscous fluid. Similarly, when air is forced into one end of a circular tube containing a viscous liquid, it forms a round-ended column or bullet-like shape which travels down the tube forcing some liquid out at the far end and leaving a fraction of the liquid m, in the form of an annular layer covering the wall. In the case of a square channel the shape of the less viscous fluid penetrating into the more viscous fluid depends on the velocity of the penetrating fluid. If the velocity of the penetrating fluid (called the bubble or finger hereafter) is larger than a certain limiting value, the bubble assumes a bullet-like shape; otherwise, the bubble conforms to the shape of the square channel. In a rectangular channel, if the capillary number, $C_A = \mu u_b/\sigma$ is not too large, a single steady-state tongue-like shape moves through the cell with constant velocity u_b, where μ is the viscosity of the driven liquid, u_b is the bubble velocity, and σ is the gas–liquid interfacial tension. In a circular tube or square channel the bullet-like shape of the bubble persists even at a very large capillary number. In other words, the fingering effect does not occur in the case of a long bubble advancing in either a circular tube or a square channel at large capillary numbers.

Fairbrother and Stubbs [20] performed the first experiments to determine the amount of liquid left inside a tube when it is displaced by another immiscible fluid. They determined the flow rate of the liquid by measuring the motion of the gas interface in the tube. When the tube is not completely filled with the liquid, the gas interface will move faster than the average velocity of the liquid due to the deposition of a thin film of liquid on the walls of the tube and if the tube is long enough, it will blowout somewhere within the tube. An empirical correlation for the fraction of the liquid deposited on the walls of the tube was formulated as follows:

$$m = \frac{(u_b - u)}{u_b} = 1.0 C_A^{1/2} = \left(\frac{\mu u_b}{\sigma}\right)^{1/2}$$

This result was found satisfactory for capillary numbers between 10^{-3} and 10^{-2}.

Isothermal gas-assisted displacement of Newtonian liquids in circular tubes was also experimentally studied by Taylor [1]. By plotting the fraction of the liquid as a

[*]Corresponding author.

[1]Present address: Department of Chemical Engineering, Faculty of Engineering, University of Firat, 23279 Elaziğ, Turkey.

1385-8947/99/$ – see front matter
PII: S1385-8947(99)00088-1

function of the capillary number, he collapsed the data on to a single curve, and showed that this fraction asymptotically approached the value of 0.56 for a capillary number nearly equal to 2. Cox [5,6] extended Taylor's [1] result to capillary numbers up to 10 and showed that the limiting fraction of the liquid deposited on the walls of the tube was approximately 0.6. His theoretical analysis resulted in a fourth-order differential equation in terms of the stream function. Inertial and gravitational forces were neglected. The streamlines were assumed to be a specific function of the spatial coordinates. The governing equations were expressed in matrix form and solved numerically.

Bretherton [2] also undertook a theoretical analysis of this problem for circular capillaries. He found an approximate solution to this problem for a circular cross-section by the method of matched asymptotic expansions. The idea behind this theoretical treatment is that for sufficiently small C_A the viscous stresses appreciably modify the static profile of the bubble only very near to the wall. In this region the lubrication approximation gives a good description of the flow field and of the interface profile. In the center of the capillary, the static profile is valid and there is a region of overlap in which the two solutions are matched. Using *the lubrication approximation* which requires quasi-unidirectional flow in the thin liquid film and assuming the slope of the fluid–fluid interface to be small, it can be shown that the velocity profile is parabolic. The boundary conditions for steady flow are the no slip condition at the capillary wall, and tangential stress equal to zero at the fluid interface. The bubble is assumed to be inviscid resulting in a constant pressure within the bubble. The pressure in the liquid film is given by the pressure drop across the interface which is approximated by the Young–Laplace equation. Bretherton [2] also systematically explored a number of possible causes for the discrepancy between the analysis and experimental data. However, none of these could provide a satisfactory explanation. Schwartz et al. [24] theoretically and experimentally considered the same problem and found some differences in liquid film thickness for sufficiently long bubbles, as compared to short bubbles.

Another experimental study by Marchessault and Mason [22] used air bubbles in a dilute aqueous solution of potassium chloride. Film thicknesses were inferred from resistance measurements and were found to be substantially larger than those reported by Bretherton [2]. The residual wetting layer of the displaced liquid will vary with the velocity of advance of the interface. Park and Homsy [3] theoretically demonstrated that the two-dimensional version of the Bretherton [2] problem is an appropriate local solution to describe the phenomenon in terms of determining residual liquid film thickness and pressure drop across the bubble front.

Ratulowski and Chan [10] theoretically and experimentally investigated a single discrete bubble and the motion of a long bubble in a circular tube and square channel. They determined the fraction of liquid deposited on the walls of the tube or channel and the pressure drop across the bubble front. According to their study, a single isolated bubble resembles an infinitely long bubble in terms of determining the film thickness and pressure drop across the bubble front if the length of the bubble exceeds the channel width. Their analysis is only valid for $C_A > 3 \times 10^{-3}$.

Kolb and Cerro [17] studied the isothermal gas-assisted displacement of a Newtonian liquid from a channel of square cross-section and showed that the liquid deposited on the wall of the square tube also approaches an asymptotic limit (0.64) at high capillary numbers. Above $C_A = 0.1$ the gas forms a circular hollow core and thicker liquid deposition; below $C_A = 0.1$ the hollow core takes on the square cross-section of the tube as the deposition thickness is reduced. The above study was extended (Kolb and Cerro [11]) by adding the lubrication approximation for intermediate to large capillary numbers where the flow is axisymmetric. In their work the film thickness on the walls of the square channel can be predicted as a function of capillary number since the velocity profile of the fluid flowing between the bubble and the square channel walls is known. It was claimed that the lubrication approximation solution is in good agreement with experimental data for values of capillary number between 0.7 and 2.0.

Unlike previous investigators, Huzyak and Koelling [9] experimentally investigated the gas-assisted displacement of non-Newtonian fluids deposited on the walls of a tube. They examined the effect of fluid elasticity and tube diameter on the fractional coverage. They concluded that unlike Newtonian fluids, the fractional coverage for viscoelastic fluids did not reach an asymptotic value but continued to increase, attaining a value in excess of 0.73, and that the fractional coverage of the viscoelastic fluids decreases with increasing tube diameter.

Ro and Homsy [4] performed an asymptotic analysis of the gas-assisted displacement of a non-Newtonian fluid in a Hele–Shaw cell. The effects of normal stress and shear stress thinning in determining the film thickness and the pressure jump across the interface were examined. Viscoelastic fluids were modeled by an Oldroyd-B constitutive equation and the solutions for the constant film thickness region and the static meniscus region were matched in the transition regime as for the Newtonian case (see Park and Homsy [3]).

The planar geometry or Hele–Shaw cell consists of two closely-separated parallel plates having a distance $2d$ between them. The sides of this rectangular channel are at a distance $2Z_o$ apart where $d \ll Z_o$. A parameter λ is defined as (thickness of gas bubble)/(distance between the plates). For the cylindrical tube λ is defined as (diameter of the bubble)/(diameter of the tube). In the rectangular channel the thickness of the tongue-like shape is $2\lambda d$ and its width is $2\lambda_w Z_o$, where the parameter λ_w is equal to (width of the bubble)/(width of the rectangular channel).

The determination of the value of λ and λ_w has been a subject of much interest. The determination of λ_w as a

function of capillary number, C_A, for different cell aspect ratios, Z_o/d, has been examined experimentally by Saffman and Taylor [26], Pitts [23], and Tabeling et al. [25]. Saffman and Taylor [26] and Pitts [23] found that the value of λ_w decreases monotonically to 0.5 when the bubble velocity is increased. In contrast, Tabeling et al. [25] reported that the value of λ_w never decreases to 0.5 when the bubble velocity is increased. The problem was reconsidered by McLean and Saffman [21] by including surface tension effects due to the lateral curvature of the interface of the advancing finger. In their numerical study the value of λ_w was close to 0.5 at large bubble velocity which is in good agreement with the experimental data. At low velocities (i.e. $C_b = 12\ C_A(Z_o/d)^2 < 100$), the agreement with experiment was poor since the finger sizes predicted by the theory were significantly below those actually measured. They found that the incorporation of surface tension and cell aspect ratio did not remedy or reduce the disagreement between theory and experiment in terms of calculating the value of λ_w as a function of C_b. The approach of Bretherton [2] was reconsidered by Park and Homsy [3] in the horizontal Hele–Shaw cell at very low capillary number. The problem was solved using a perturbation method with an asymptotic expansion of $C_A^{1/3}$ and the ratio of the gap width to the transverse characteristic length $\delta_e = d/Z_o$ as small quantities. They obtained relationships between λ, C_A, and δ_e for calculating the film thickness and pressure jump across the bubble front. The resulting expressions were compared with the results of Bretherton [2] and Landau and Levich [16] and were considered to give improved results.

Reinelt [7] extended his earlier work by determining the perturbation solution of the axisymmetric flow problem for small values of C_A and $\delta = d/Z_o$. In his study, some of the boundary conditions were improved by incorporating the film thickness into the kinematic boundary condition and taking into account the dependence of Δp on the capillary number. The problem was also numerically solved using a conformal mapping method and the numerical results were presented in another paper (Reinelt [12]). Although the inclusion of the effects of the film thickness variation and the lateral and transverse curvature on the interface boundary conditions improved the quantitative agreement between the experimental and numerical results, it did not remove the discrepancy associated with different finger widths.

In this paper the gas assisted displacement of a power-law fluid in a tube or a rectangular channel was studied analytically using a singular perturbation method. Also the problem is examined experimentally in order to determine the effect of non-Newtonian fluid rheology such as shear thinning on the liquid fraction deposited on the wall as a function of capillary number (see Kamişli [8]). However, the experimental results are not presented here except the residual liquid film thickness of Newtonian and some non-Newtonian fluids as a function of capillary number.

2. Experimental

The experimental arrangement consists of a gas supply tank, pressure transducer, transparent plastic or glass tubes/channels and associated valves and fittings as shown in Fig. 1. The volume of the gas supply tank was chosen to be very large in comparison to the volume of the gas within the tube or channel in order to minimize pressure fluctuations during the experiments. Pressurized air was used as the gas and was supplied by a local compressed air line and monitored with a pressure gauge mounted on the tank. The desired pressure level can be accurately adjusted by keeping valve B open and D closed and reading the pressure from the pressure transducer for a particular setting of valve C. The line pressure is also independently measured using a pressure transducer situated close to the channel assembly. Plastic or glass tubes having a diameter 4.763 mm and a length of 50 cm were used. Caliper measurements showed that the inner radius along the tube length had a maximum variation of ± 0.065 mm.

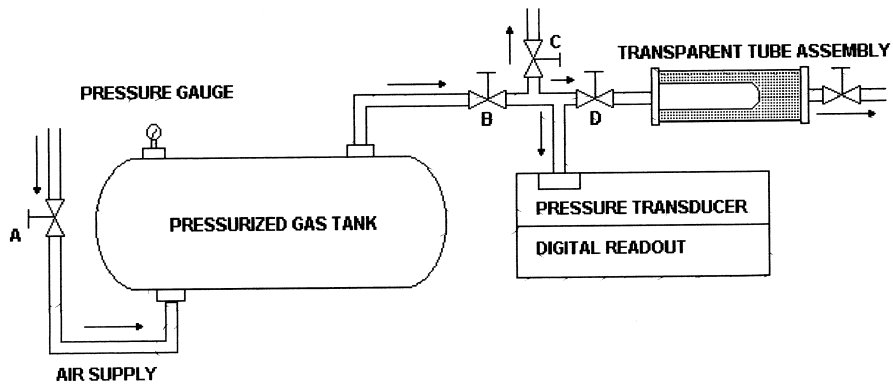

Fig. 1. Schematic diagram of the experimental apparatus.

Isothermal experiments have been conducted to measure the displacement of the gas–liquid interface as a function of the applied pressure differential. The velocity of the interface and the residual liquid film thickness have been determined for Newtonian, non-Newtonian, and viscoelastic liquids (see Kamişli [8] for details). Viscosity was measured using a Haake Rotovisco (Model RV12) as well as a calibrated glass capillary viscometer. The dimensionless groups are based on the power-law parameters evaluated from the viscometric data obtained in the Haake viscometer ($K = 58.75$ (Pa s^n) and $n = 0.485$ for 1% HEC, and $K = 2.85$ (Pa s^n) and $n = 0.652$ for 1% CMC). Experiments were performed in two types of tube arrangement namely open tubes and valve-mounted closed tubes. In the tube open to the atmosphere, the tube was initially filled with liquid to a distance of 15 cm. The end of the tube was open to the atmosphere. The velocity of the gas bubble and displaced liquid were determined using a stop-watch and observed positions of the gas–liquid interface. The moving bubble attained its final shape within a few diameters of the gas injection point and translated unchanged along the length of the tube. The velocity of the gas bubble and the velocity of the liquid displaced by the gas are dependent upon how much liquid there is between the nose of the bubble and the moving liquid front.

On the other hand, the valve-mounted closed tubes result in a uniform bubble velocity since the flow resistance of the fluid in the channel is negligible when compared with the resistance valve. In this type arrangement experiments were conducted using a completely filled tube having 4.763 mm diameter, 50 cm length, and a valve at the one end. The valve provides much more resistance than that of liquid flow. Thus, a uniform bubble velocity along the axial direction was obtained. The maximum variation in the bubble velocity was found to be less than 5% for most of the test fluids. The capillary numbers were calculated from the average bubble velocity. In this case, the fraction of liquid deposited on the tube wall was calculated by weighing the liquid expelled by the long gas bubble since the initial amount of liquid within the tube is known from the liquid density, tube diameter, and length.

In this paper, the results of valve-mounted closed tubes are presented in order to compare with the results of an analysis of a singular perturbation method for low capillary numbers.

3. Results of experiment

The fraction of the liquid deposited on the wall of the tube for the different liquids is plotted in Fig. 2 as a function of the capillary number for a particular tube diameter of 4.763 mm. The experimental data for the Newtonian fluid are in close agreement with Taylor's [1] experimental data as can be seen in Fig. 2. Taylor used corn syrup as a Newtonian fluid and collapsed the data on to a single curve

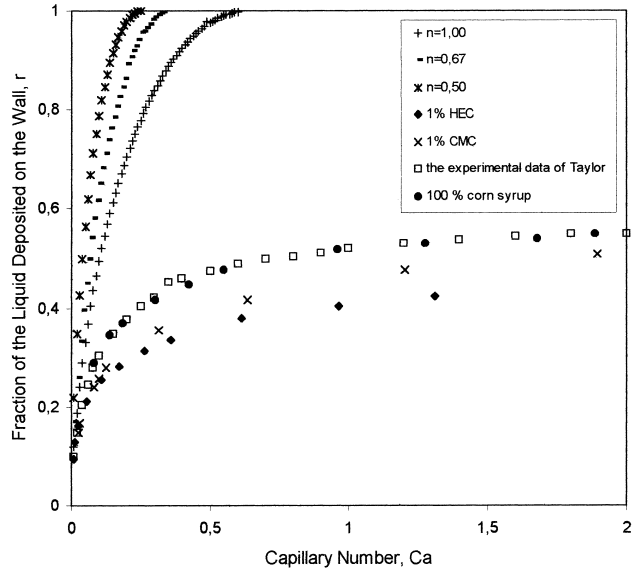

Fig. 2. The results of perturbation analysis for various values of power-law index n and the experimental data for Newtonian and non-Newtonian fluids deposited on the walls of the tube as a function of capillary number.

and showed that the fraction of the liquid deposited on the wall asymptotically approached the value of 0.56 for a capillary number nearly equal to 2. Different capillary numbers for each tube are obtained by changing the pressure of the gas. Each experiment was repeated six times in order to check repeatability. The coating of the liquid on the walls of the tube depends primarily on how fast the gas moves through the liquid. Increasing gas pressure, larger radii and lower viscosity reduce the flow resistance and result in higher bubble velocity and higher residual liquid film thickness on the tube wall.

4. Perturbation method

The gas-assisted displacement process can be considered as a singular perturbation problem. This approach for the case of a Newtonian fluid was first provided by Bretherton [2] by means of a perturbation expansion in $C_A^{1/3}$. Later Park and Homsy [3] and Reinelt [7] expanded the solution in both $C_A^{1/3}$ and $\delta = b/d$ and made some improvement in determining the film thickness and the pressure at the nose of the bubble. Recently the same method was applied by Ro and Homsy [4] for a viscoelastic (Oldroyd-B) fluid.

In the perturbation method it is assumed that the bubble is moving with a sufficiently small value of the capillary number C_A and the interface is almost parallel to the wall of the tube or channel. Thus, the fluid motion in this region can be treated as if the region were planar and not annular. The solution for the film thickness is therefore valid for both two-dimensional and axisymmetric flow. Therefore the subsequent analysis employs the continuity equation and equation of motion for two-dimensional flow. Inner and

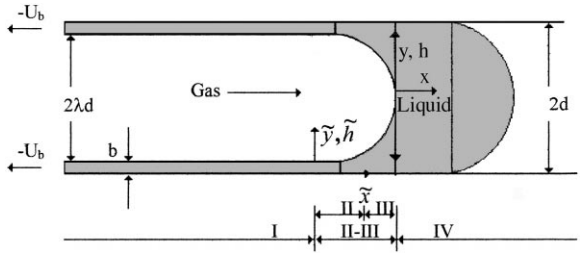

Fig. 3. Schematic diagram of gas-assisted displacement for different regions (II: transition region, III: capillary static region).

outer expansions are developed in terms of a small parameter $C_A^{1/3}$ for a non-Newtonian fluid. The method of matched asymptotic expansions is used to match the inner and outer solutions (Nayfeh [19] and Van Dyke [18]).

In this analysis, the origin of the frame of reference is taken to be the nose of the bubble which is moving in the positive x-direction.

Consider the motion of a gas bubble into an incompressible Newtonian or non-Newtonian liquid as shown schematically in Fig. 3. For convenience, velocities are non-dimensionalized by the uniform velocity u_b, the transverse and axial coordinates by the characteristic length d, and the pressure by σ/d. The characteristic length d is taken to be either the radius of the tube or half of the distance between the parallel plates. The equation of continuity and motion are given as follows:

$$\frac{1}{\dot{y}^a}\frac{\partial}{\partial \dot{y}}(\dot{y}^a \dot{u}) + \frac{\partial \dot{v}}{\partial \dot{x}} = 0 \tag{1}$$

$$\rho\left(\frac{\partial \dot{v}}{\partial \dot{t}} + \dot{v}\frac{\partial \dot{v}}{\partial \dot{x}} + \dot{u}\frac{\partial \dot{v}}{\partial \dot{y}}\right) = -\frac{\partial \dot{p}}{\partial \dot{x}} - \left[\frac{1}{\dot{y}^a}\frac{\partial}{\partial \dot{y}^a}(\dot{y}^a \tau_{yx}) + \frac{\partial \tau_{xx}}{\partial \dot{x}}\right] \tag{2}$$

$$\rho\left(\frac{\partial \dot{u}}{\partial \dot{t}} + \dot{v}\frac{\partial \dot{v}}{\partial \dot{x}} + \dot{u}\frac{\partial \dot{u}}{\partial \dot{y}}\right) = -\frac{\partial \dot{p}}{\partial \dot{y}} - \left[\frac{1}{\dot{y}^a}\frac{\partial}{\partial \dot{y}^a}(\dot{y}^a \tau_{yy}) + \frac{\partial \tau_{xy}}{\partial \dot{x}}\right] \tag{3}$$

The parameter a has a value of either 0 or 1 depending on the geometry (0 corresponds to the planar case and 1 corresponds to a cylindrical geometry). τ_{ij} is the stress tensor and $\dot{p}$ is the pressure. The velocity components $\dot{v}$ and $\dot{u}$ are in the $\dot{x}$ and $\dot{y}$ directions, respectively. The $\dot{y}$ axis is taken normal to the channel plates (or tube wall) with the origin at the mid-plane (or tube axis). Thus $\dot{y}$ has the value of $\pm d$ for the planar case (or d for the cylindrical case) at the solid boundaries. The origin is assumed to be located at the nose of the bubble and consequently the velocity is independent of time with respect to this frame of reference. Dimensionless variables are defined as follows:

$$x = \frac{(\dot{x} - u_b t)}{d}, \quad y = \frac{\dot{y}}{d}, \quad H = \frac{\dot{H}}{d}$$

$$v = \frac{\dot{v}}{u_b}, \quad u = \frac{\dot{u}}{u_b}, \quad p = \frac{\dot{p}}{(\sigma/d)}$$

In this analysis, a power-law model is considered where the viscosity is defined as

$$\dot{\mu} = K\left(\frac{1}{2}II_\Delta\right)^{((n-1)/2)}$$

where II_Δ is the second scalar invariant. The viscosity in dimensionless form becomes

$$\dot{\mu} = K\left(\frac{u_b}{d}\right)^{n-1}\left[2\left(\frac{\partial \dot{v}}{\partial \dot{x}}\right)^2 + \left(\frac{\partial \dot{u}}{\partial \dot{x}} + \frac{\partial \dot{v}}{\partial \dot{y}}\right)^2 + 2\left(\frac{\partial \dot{u}}{\partial \dot{y}}\right)^2\right]^{((n-1)/2)}$$

$$\dot{\mu} = M\mu$$

where $M = K(u_b/d)^{(n-1)}$ can be considered as the apparent viscosity at a (nominal) shear rate of (u_b/d) and μ is

$$\left[2\left(\frac{\partial \dot{v}}{\partial \dot{x}}\right)^2 + \left(\frac{\partial \dot{u}}{\partial \dot{x}} + \frac{\partial \dot{v}}{\partial \dot{y}}\right)^2 + 2\left(\frac{\partial \dot{u}}{\partial \dot{y}}\right)^2\right]^{((n-1)/2)}$$

By taking $a = 0$ Equations (1)–(3) can be expressed in dimensionless form as

$$\frac{\partial u}{\partial y} + \frac{\partial v}{\partial x} = 0 \tag{4}$$

$$\frac{\partial p}{\partial y} = C_A\left[2\frac{\partial}{\partial x}\left(\mu\frac{\partial v}{\partial x}\right) + \frac{\partial}{\partial y}\left(\mu\left(\frac{\partial u}{\partial x} + \frac{\partial v}{\partial y}\right)\right)\right] \tag{5}$$

$$\frac{\partial p}{\partial y} = C_A\left[\frac{\partial}{\partial x}\left(\mu\left(\frac{\partial u}{\partial x} + \frac{\partial v}{\partial y}\right)\right) + 2\frac{\partial}{\partial y}\left(\mu\frac{\partial u}{\partial y}\right)\right] \tag{6}$$

where $C_A = Mu_b/\sigma$ may be regarded as a modified capillary number and $Re/C_A = (d\rho/M)\,(\sigma/M)$ was taken to be less than unity. In this analysis, the no-slip condition is applied on the solid boundaries. In order to establish the appropriate interfacial conditions, it is assumed that the viscosity of the gas within the bubble is negligible when compared with the viscosity of the fluid exterior to the bubble. It is also assumed that the displaced non-Newtonian liquid wets the walls of the tube or channel and leaves a film of uniform thickness on the walls. Shear stress thinning is described by the power-law model. In this analysis the problem is solved using a perturbation method in an expansion of the modified capillary number in powers of $C_A^{1/3}$.

The kinematic boundary condition at the interface is given by

$$\frac{dy}{dx} = \frac{u}{v} \tag{7}$$

The tangential stress boundary condition at the interface is independent of frame of reference and is given by

$$\tau_{yy}n_y t_y + \tau_{xy}n_x t_y + \tau_{yx}n_y t_x + \tau_{xx}n_x t_x = 0 \tag{8}$$

The difference in the normal stress on the two sides of the interface is balanced by surface tension and is expressed as

$$\tau_{yy}n_y^2 + \tau_{yy}n_x^2 + 2\tau_{yy}n_x n_y = -p_0 + \frac{\sigma}{\dot{R}} \tag{9}$$

where τ is the total stress tensor, and n and t are unit vectors normal and tangent to the interface, respectively and subscript x and y denote their components. Also $\dot{R}$ is the principal radius of curvature of the interface and p_0 is the pressure within the gas bubble.

Substituting the stress tensor and the expressions for n_x and n_y into Eqs. (8) and (9) gives

$$\left[-2\frac{\mathrm{d}y}{\mathrm{d}x}\left(v_x-u_y\right)+\left\{1-\left(\frac{\mathrm{d}y}{\mathrm{d}x}\right)^2\right\}\left(u_x+v_y\right)\right]=0 \tag{10}$$

$$p=-\frac{1}{R}+2C_{\mathrm{A}}\mu\left[1+\left(\frac{\mathrm{d}y}{\mathrm{d}x}\right)^2\right]^{-1} \times\left\{\left(\frac{\mathrm{d}y}{\mathrm{d}x}\right)^2 v_x+u_y-\left(\frac{\mathrm{d}y}{\mathrm{d}x}\right)\left(u_x+v_y\right)\right\} \tag{11}$$

In order to do appropriate scaling, the flow region can be divided into four regions as shown in Fig. 3. The flow regions I, II–III, and IV represent the thin film region, the meniscus front region, and the parallel or tubular flow region, respectively. The meniscus front region can be divided into two subregions: for small C_{A}, a capillary static region (III) where the shape of the interface is almost circular and the transition region (II) where the circular shape of the interface is deformed by viscous forces and shear thinning effects. The hydrostatic, nearly circular interface in the capillary static region is due to the dominance of pressure and interfacial tension in that region. The presence of the transition region allows matching of the solution in the capillary static region to the solution in the constant film thickness region. As will be seen later, the transition region is important since shear thinning effects have the greatest impact in that region.

In order to obtain the leading order terms in the outer expansion when $C_{\mathrm{A}}\to 0$ Eqs. (5) and (6) become

$$p_x^0=0 \quad \text{and} \quad p_y^0=0$$

where the superscript (0) denotes the zeroth order approximation in the outer expansion. $p_x^0=p_y^0=0$ implies that the leading order approximation to the pressure $p_0(x, y)$ is constant. In order to determine the value of this constant, the interfacial boundary conditions have to be examined when $C_{\mathrm{A}}\to 0$. As can be seen in Eq. (11), the viscous force term goes to zero when $C_{\mathrm{A}}\to 0$ and the gas bubble fills the entire tube or channel. This implies that $\lambda\to 1$ and the radius of curvature will be equal to the radius of the tube. When $C_{\mathrm{A}}\to 0$, Eq. (11) becomes

$$p^0=-\frac{1}{R}=h_{xx}^0\left[1+\left(h_x^0\right)^2\right]^{-3/2} \tag{12}$$

In order to obtain the static meniscus, the above equation is integrated subject to the conditions

$$h_x\to\infty \quad \text{and} \quad h=0 \quad \text{at} \quad x=0$$

The solution of Eq. (12) is

$$h^0(x)=-\frac{1}{p^0}\left[1-\left(p^0x+1\right)^2\right]^{1/2} \tag{13}$$

Since the bubble fills the entire tube and the pressure is equal to the radius of curvature, the pressure must therefore be equal to 1. In the transition region, the problem has to be rescaled in order to apply *the lubrication approximation*. In this region, the pressure, viscous force, interfacial tension and shear thinning behaviour are all important. The inner variables may be rescaled in a manner similar to the Newtonian case as follows:

$$\tilde{v}=v, \quad \tilde{u}=\frac{u}{C_{\mathrm{A}}^{1/3}}, \quad \tilde{p}=p, \quad \tilde{\mu}=\mu C_{\mathrm{A}}^{(2(n-1))/3}$$

$$\tilde{x}=\frac{(x+l)}{C_{\mathrm{A}}^{1/3}}, \quad \tilde{h}=\frac{(h+l)}{C_{\mathrm{A}}^{2/3}}, \quad \tilde{y}=\frac{(y+l)}{C_{\mathrm{A}}^{2/3}}$$

The viscosity becomes

$$\tilde{\mu}=\left[2C_{\mathrm{A}}^{2/3}\left(\frac{\partial\tilde{v}}{\partial\tilde{x}}\right)^2+\left(C_{\mathrm{A}}^{2/3}\frac{\partial\tilde{u}}{\partial\tilde{x}}+\frac{\partial\tilde{v}}{\partial\tilde{y}}\right)^2+2C_{\mathrm{A}}^{2/3}\left(\frac{\partial\tilde{u}}{\partial\tilde{y}}\right)^2\right]^{(n-1)/2} \tag{14}$$

From the above Eq. (14) $\tilde{\mu}=(\partial\tilde{v}/\partial\tilde{y})^{n-1}$ when $C_{\mathrm{A}}\to 0$.

Eqs. (5) and (6) with rescaled variables are given by

$$\tilde{p}_{\tilde{x}}=\left[2C_{\mathrm{A}}^{2/3}\frac{\partial}{\partial\tilde{x}}\left(\tilde{\mu}\frac{\partial\tilde{v}}{\partial\tilde{x}}\right)+\frac{\partial}{\partial\tilde{y}}\left(\tilde{\mu}\left(C_{\mathrm{A}}^{2/3}\frac{\partial\tilde{u}}{\partial\tilde{x}}+\frac{\partial\tilde{v}}{\partial\tilde{y}}\right)\right)\right] \tag{15}$$

$$\tilde{p}_{\tilde{y}}=\left[\frac{\partial}{\partial\tilde{x}}\left(\tilde{\mu}\left(C_{\mathrm{A}}^{4/3}\frac{\partial\tilde{u}}{\partial\tilde{x}}+\frac{\partial\tilde{v}}{\partial\tilde{y}}\right)\right)+2C_{\mathrm{A}}^{2/3}\frac{\partial}{\partial\tilde{y}}\left(\tilde{\mu}\frac{\partial\tilde{u}}{\partial\tilde{y}}\right)\right] \tag{16}$$

When $C_{\mathrm{A}}\to 0$, Eqs. (15) and (16) become

$$\tilde{p}_{\tilde{x}}=\frac{\partial}{\partial\tilde{y}}\left(\tilde{\mu}\frac{\partial\tilde{v}}{\partial\tilde{y}}\right)$$

$$\tilde{p}_{\tilde{y}}=0$$

The equation of continuity and other boundary conditions are given by

$$\tilde{v}_{\tilde{x}}+\tilde{u}_{\tilde{y}}=0$$

$$\tilde{v}=-1 \quad \text{at} \quad \tilde{y}=0$$

$$\tilde{v}_{\tilde{y}}=0 \quad \text{at} \quad \tilde{y}=\tilde{h}$$

$$\tilde{u}(\tilde{x},0)=0$$

When $C_{\mathrm{A}}\to 0$, the boundary conditions with rescaled variables at the interface (Eqs. (7), (10) and (11)) at $\tilde{y}=\tilde{h}$ become

$$\tilde{u}(\tilde{x},\tilde{h})=\tilde{h}_{\tilde{x}}\tilde{v}(\tilde{x},\tilde{h})$$

$$\tilde{v}_{\tilde{y}}(\tilde{x},\tilde{h})=0$$

$$\tilde{p}(\tilde{x},\tilde{h})=\tilde{h}_{\tilde{x}\tilde{x}}$$

$$\tilde{p}(\tilde{x},\tilde{y})=\tilde{p}(\tilde{x})$$

The expansion of all unknown quantities in powers of the modified capillary number $C_A^{1/3}$ can be done as follows:

$$p(x,y) = \sum_{i=0}^{\infty} p(x,y)^i C_A^{(1/3)i}$$

$$v(x,y) = \sum_{i=0}^{\infty} v(x,y)^i C_A^{(1/3)i}$$

$$u(x,y) = \sum_{i=0}^{\infty} u(x,y)^i C_A^{(1/3)i}$$

$$h(x,y) = \sum_{i=0}^{\infty} h(x,y)^i C_A^{(1/3)i}$$

$$\mu(v,u) = \sum_{i=0}^{\infty} \mu(v,u)^i C_A^{(1/3)i}$$

Substituting these expansions into the above expressions gives the zeroth order approximation as follows at $\tilde{y} = \tilde{h}^0(\tilde{x})$

$$\tilde{u}^0(\tilde{x},\tilde{h}^0) = \tilde{h}^0_{\tilde{x}}\tilde{v}^0(\tilde{x},\tilde{h}^0) \tag{17}$$

$$\tilde{v}^0_{\tilde{y}}(\tilde{x},\tilde{h}^0) = 0 \tag{18}$$

$$\tilde{p}^0(\tilde{x},\tilde{h}^0) = \tilde{h}^0_{\tilde{x}\tilde{x}} \tag{19}$$

$$\tilde{p}^0_{\tilde{x}} = \frac{\partial}{\partial\tilde{y}}\left(\tilde{\mu}\frac{\partial\tilde{v}^0}{\partial\tilde{y}}\right) \tag{20}$$

$$\tilde{p}_{\tilde{y}} = 0 \tag{21}$$

$$\tilde{v}^0_{\tilde{x}} + \tilde{u}^0_{\tilde{y}} = 0 \tag{22}$$

$$\tilde{v}^0(\tilde{x},0) = -1$$

$$\tilde{u}^0(\tilde{x},0) = 0$$

As in the Newtonian case, a third-order differential equation in h may be obtained from Eqs. (17), (19), (20) and (22). From Eq. (20)

$$\tilde{v}^0 = \frac{(\tilde{p}^0_{\tilde{x}})^{\alpha}}{\alpha+1}\left[-\left(-\tilde{y}+\tilde{h}^0\right)^{\alpha+1} + \left(\tilde{h}^0\right)^{\alpha+1}\right] - 1 \tag{23}$$

where $\alpha = 1/n$. Eq. (23) is subject to the boundary conditions $\tilde{v}^0_{\tilde{y}}(\tilde{x}) = 0$ at $\tilde{y} = \tilde{h}$ and $\tilde{v}^0 = -1$ at $\tilde{y} = 0$.

From Eqs. (17), (22) and (23) with the given boundary conditions the following equation was obtained.

$$-\tilde{h}^0_{\tilde{x}} = -\frac{\alpha}{\alpha+1}\tilde{p}^0_{\tilde{x}\tilde{x}}\left(\tilde{p}^0_{\tilde{x}}\right)^{(\alpha-1)}\left(\tilde{h}^0\right)^{(\alpha+2)} - \left(\tilde{p}^0_{\tilde{x}}\right)^{\alpha}\left(\tilde{h}^0\right)^{(\alpha+1)}\tilde{h}^0_{\tilde{x}} \tag{24}$$

Integrating Equation (24) and taking the derivative of Eq. (19) with respect to x and substituting gives

$$\tilde{h}^0_{\tilde{x}\tilde{x}\tilde{x}} = \left[\frac{(\alpha+2)(\tilde{h}^0-\tilde{b})}{(\tilde{h}^0)^{\alpha+2}}\right]^{1/\alpha} \tag{25}$$

The integration constant is obtained from the condition $\tilde{h}^0 = b$ as $\tilde{x}\to-\infty$.

Since Eq. (25) is an ordinary differential equation, it can be solved numerically. Eq. (25) can be expressed in translation form since it is an autonomous equation. The following transformation is introduced

$$X = \frac{(\alpha+2)^{1/3\alpha}(\tilde{x}+\tilde{x}_0)}{\tilde{b}^{(1+2\alpha)/3\alpha}} \quad \text{and} \quad H = \frac{\tilde{h}^0}{\tilde{b}}$$

With this transformation Eq. (25) becomes

$$H_{XXX} = \left[\frac{H-1}{H^{\alpha+2}}\right]^{1/\alpha} \tag{26}$$

Since Eq. (26) is a third-order equation, the solution will contain three constants. It is expected that two of these three constants have to be discarded because they are associated with terms that grow exponentially when $\tilde{x}\to\infty$ as in the Newtonian case. Although the fluid is non-Newtonian, the Newtonian approximation can be used for the initial conditions because the shape of the interface can be expressed in exponential and quadratic form according to the region ($H \to 1$ as $X\to-\infty$ for both the Newtonian and non-Newtonian case). Therefore identical initial conditions to the Newtonian case are used in order to integrate Eq. (26) numerically. The constants of the quadratic equation are obtained from numerical integration of Eq. (26) as a function of the initial conditions. When $X\to-\infty$, the solution becomes independent of α, $H\to1$ and the solution of Eq. (26) can be expressed as follows:

$$H = AX^2 + BX + C \tag{27}$$

Table 1 is obtained using the same initial conditions for each value of α in conjunction with Eq. (27), where A, B, and C are the curvature coefficients.

The inner solution and outer solution have now been determined in terms of h. The inner and outer solutions have to match somewhere in the transition region. The asymptotic matching is accomplished at $\tilde{x}\to\infty$ for the inner solution and at $\tilde{x}\to-l$ for the outer solution. The inner solution, Eq. (27) is expressed in terms of the original variables as

Table 1
Constants of Eq. (27) as a function of power-law index

α	1.00	1.25	1.50	2.00	3.00	4.00	5.00
A	0.3215	0.4042	0.4732	0.5806	0.7212	0.8083	0.8689
B	0.0737	2.4482	4.2366	6.7329	9.5743	11.1068	12.0215
C	2.8348	6.9668	13.3160	26.0125	43.8635	63.2813	88.2046

$$\tilde{h}^0 = -1 + \left[\frac{A\tilde{b}(\alpha+2)^{2/3\alpha}}{\tilde{b}^{2(1+2\alpha)/3\alpha}}\right](x+l)^2 + C_A^{1/3} \times \left[\frac{2A\tilde{b}(\alpha+2)^{2/3\alpha}}{\tilde{b}^{2(1+2\alpha)/3\alpha}}\tilde{x}_0 + \frac{B\tilde{b}(\alpha+2)^{1/3\alpha}}{\tilde{b}^{2(1+2\alpha)/3\alpha}}\right](x+l) + C_A^{2/3} \times \left[\frac{A\tilde{b}(\alpha+2)^{2/3\alpha}}{\tilde{b}^{2(1+2\alpha)/3\alpha}}\tilde{x}_0^2 + \frac{B\tilde{b}(\alpha+2)^{1/3\alpha}}{\tilde{b}^{(1+2\alpha)/3\alpha}}\tilde{x}_0 + \tilde{b}C\right] \quad (28)$$

The value of l can be determined from Eq. (13) with the matching condition $h^0 \to -1$ as $\tilde{x} \to -l$. This implies $l = 1$ and Eq. (13) may be expressed using a Taylor series expansion as

$$h^0(x) = -[1 - \tfrac{1}{2}(x+1)^2 + 0((x+1)^4)] \quad (29)$$

Comparing Eq. (29) with Eq. (28), the asymptotic matching to $O(C_A^0)$ gives

$$\tilde{b} = \left[2A(\alpha+2)^{2/3\alpha}\right]^{3\alpha/\alpha+2}$$

In order to match other terms in the inner expansion, a higher-order expansion is required for the outer solution. This can be done by substituting a higher-order expansion of the variables in powers of $C_A^{1/3}$ into Eq. (11).

It can be seen that the viscous terms will not contribute until powers of $O(C_A)$ when the higher-order expansion of the variable in powers of $C_A^{1/3}$ is substituted into Eq. (11). This means that p^1 and p^2 are constant and equal to the radius of curvature. Therefore p^1 and p^2 are

$$p^1 = h_{xx}^1\left[1 + (h_x^0)^2\right]^{-3/2} - 3h_x^1 h_x^0 h_{xx}^0\left[1 + (h_x^0)^2\right]^{-5/2} \quad (30)$$

$$p^2 = h_{xx}^2\left[1 + (h_x^0)^2\right]^{-3/2} - 3\left(h_x^1 h_x^0 h_{xx}^1 + h_x^0 h_x^2 h_{xx}^0 + \tfrac{1}{2}(h_x^1)^2 h_x^0\right) \times \left[1 + (h_x^0)^2\right]^{-5/2} \quad (31)$$

The solution of Eq. (30) is

$$h^1(x) = -p^1 x\left[1 - (x+1)^2\right]^{-1/2} \quad (32)$$

A Taylor series expansion of Eq. (32) about $x \to -1$ gives

$$h^1(x) = p^1 - p^1(x+1) + 0\left((x+1)^2\right) \quad (33)$$

If Eq. (33) is compared with Eq. (28) to powers of $O(C_A^{1/3})$, it can be found that p^1 must be equal to zero. Therefore $\tilde{x}_0$ can be calculated from this matching condition which is

$$\tilde{x}_0 = -\frac{\tilde{b}^{(1+2\alpha)/3\alpha}B}{2A(\alpha+2)^{1/3\alpha}}$$

Since h^1 is equal to zero from the matching to powers of $O\left(C_A^{1/3}\right)$, Eq. (31) becomes

$$p^2 = h_{xx}^2\left[1 + (h_x^0)^2\right]^{-3/2} - 3\left(h_x^0 h_x^2 h_{xx}^0\right)\left[1 + (h_x^0)^2\right]^{-5/2} \quad (34)$$

The solution of Eq. (34) is

$$h^2(x) = -p^2 x\left[1 - (x+1)^2\right]^{-1/2} \quad (35)$$

A Taylor series expansion of Eq. (35) about $x \to -1$ gives

$$h^2(x) = p^2 - p^2(x+1) + 0\left((x+1)^2\right) \quad (36)$$

Comparing Eq. (36) with Eq. (28) in terms of powers of $C_A^{2/3}$ gives

$$p^2 = \frac{A\tilde{b}(\alpha+2)^{2/3\alpha}}{\tilde{b}^{2(1+2\alpha)/3\alpha}}\tilde{x}_0^2 + \frac{B\tilde{b}(\alpha+2)^{1/3\alpha}}{\tilde{b}^{(1+2\alpha)/3\alpha}}\tilde{x}_0 + \tilde{b}C$$

The following relationships are obtained up to powers of $O\left(C_A^{2/3}\right)$ as $\tilde{x} \to \infty$ and $x \to -1$.

$$\lambda = 1 - \tilde{b}C_A^{2/3}$$

$$p = 1 + p^2 C_A^{2/3}$$

$$h = -1 + p^2 C_A^{2/3} \quad (37)$$

Since the expansions are up to powers of $O\left(C_A^{1/3}\right)$, Eq. (37) is unfortunately valid only for very small values of the modified capillary number C_A.

5. Results and discussion

The values of λ were calculated analytically as a function of the modified capillary number, C_A, by varying the power-law index, n. The results are shown in Fig. 4. As can be seen in the figure, the values of λ, as a function of C_A, decrease with decreasing power-law index. In other words, the liquid film thickness increases with decreasing power-law index. Also, the valid range of the method decreases with decreasing power-law index.

Although the perturbation analysis provides reasonable agreement with experimental data over a small range of capillary number (see Bretherton [2]) for a Newtonian fluid, it does not provide the same agreement between experiment and theory for non-Newtonian fluids. In the perturbation method λ may be calculated from the following expression for the case of a non-Newtonian fluid.

$$\lambda = 1 - \tilde{b}C_A^{2/3} \quad \text{and} \quad \tilde{b} = \left[2A(\alpha+2)^{2/3\alpha}\right]^{3\alpha/\alpha+2}$$

Therefore the fraction of liquid deposited on the walls is given by

$$m = \tilde{b}C_A^{2/3} \quad \text{for rectangular channel}$$

$$m = 2\tilde{b}C_A^{2/3} - (\tilde{b})^2 C_A^{4/3} \quad \text{for a circular tube}$$

As shown in the above expressions the residual liquid film thickness depends on the values of A and the power-law index, n, as graphically shown in Fig. 5. In Fig. 5 the values of A increase with decreasing power-law index, thereby the

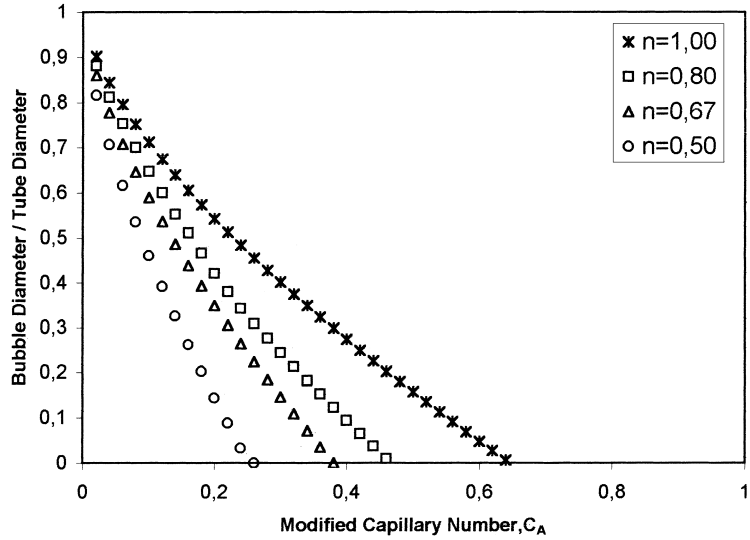

Fig. 4. Effect of the power-law index n on the liquid film thickness for perturbation solution.

liquid film thickness increases with decreasing power-law index. Thus, the theory presented here is inadequate for prediction of the absolute magnitude of film thickness for a power-law fluid.

It can be considered that the deviations between theory and experiment for power-law fluids are due to inaccurate values of the curvature coefficient, A. The reason for these deviations is a matching between the entrained film and the static meniscus at different, rather than equal, values of H (∞ and 1). In other words, the assumptions made in solving Eq. (26).

This problem can be understood by examining the convergence of d^2H/dX^2 as $H \rightarrow \infty$ for two extreme cases: $n = 1$, Newtonian case, and $n \rightarrow 0$. Eq. (26) in terms of n becomes

$$\frac{d^3H}{dX^3} = \frac{(H-1)^n}{H^{2n+1}}$$

For $n = 1$:

$$\lim_{H\rightarrow\infty} \frac{d^3H}{dX^3} = \lim_{H\rightarrow\infty} \frac{H-1}{H^3} = \lim_{H\rightarrow\infty} \frac{1}{H^2} \rightarrow 0 \qquad (38)$$

For $n = 0$:

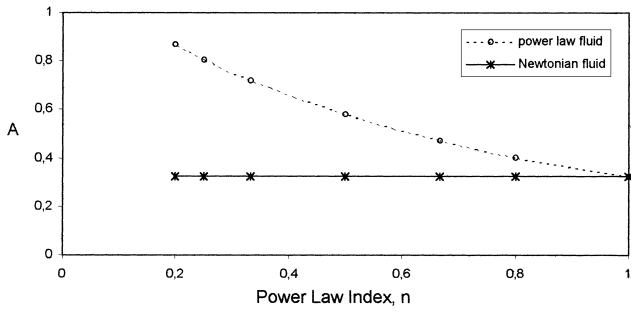

Fig. 5. Variation of the curvature coefficient, A with power-law index, n.

$$\lim_{H\rightarrow\infty} \frac{d^3H}{dX^3} = \lim_{H\rightarrow\infty} \frac{(H-1)^n}{H^{2n+1}} = \lim_{H\rightarrow\infty} \frac{1}{H} \rightarrow 0 \qquad (39)$$

Eqs. (38) and (39) show that while both third derivatives converge to zero, the rate of convergence is different. In the case of $n = 0$, the convergence is considerably slower. Therefore, for values of n less than 1, the second derivative becomes constant only at a higher H and the value of A is higher as is evidenced in Table 1. As a result m will be higher than for $n = 1.0$.

As mentioned earlier, the perturbation solution is valid only for very low capillary numbers; therefore a direct comparison of the experimental data with the theoretical results should be made with caution even though the experimental data, in general, show that the fraction of the liquid deposited on the tube wall increases with decreasing values of power-law index.

Ro and Homsy [4] solved the two-dimensional flow in a Hele-Shaw cell containing a viscoelastic (Oldroyd-B) fluid using an expansion in $C_A^{1/3}$ and We. Their theoretical analysis allowed them to conclude that the film thickness decreases and pressure drop at the meniscus tip increases as the fluid becomes more viscoelastic. In the present analysis, the residual liquid film thickness increases with decreasing power-law index. Thus, the trend observed for a perturbation using a power-law constitutive equation differs from that of Ro and Homsy's [4] perturbation analysis.

When the origin of the frame of reference is taken to be the nose of the bubble, the gas-assisted displacement problem in terms of determining the residual liquid film thickness on the wall becomes very similar to the free coating of a vertically withdrawn plate from the liquid reservoir. The results of this analysis for non-Newtonian fluids were compared with the experimental results of the free coating of a vertically withdrawn plate from a non-Newtonian fluid reservoir.

According to the singular perturbation method non-Newtonian fluids give a higher residual liquid film thickness than for a corresponding Newtonian fluid although the experimental results by Tallmadge [13,14] and Spiers et al. [15] showed that the residual liquid film thickness of non-Newtonian fluids on a vertically withdrawn plate from a liquid reservoir is smaller than that of Newtonian fluids. However, these results were not observed in theoretical analysis by Tallmadge [13,14].

On the other hand, it was experimentally observed that the fraction of the liquid deposited on the tube wall for Newtonian and non-Newtonian fluids is almost identical at low capillary number (see Fig. 2). In other words, low capillary number gas-assisted non-Newtonian fluid displacement shows similar behaviour to Newtonian fluid displacement at low capillary number. A similar trend was observed using a perturbation analysis for a power-law constitutive equation at low capillary number. As can be seen in Fig. 4 the effect of the power-law index on values of λ was not very pronounced at low capillary number. In other words, at low capillary number the residual liquid film thickness of power-law fluids is almost independent of the value of power-law index.

6. Conclusions

A perturbation analysis using a power-law constitutive equation does not correctly predict the variation of the residual liquid film thickness as a function of the power-law index. The residual liquid film thickness is predicted to increase with decreasing power-law index which is opposite to the experimental observation of previous investigators. However it was experimentally observed that the fraction of the liquid deposited on the tube wall for Newtonian and non-Newtonian fluids is almost identical at low capillary number. Using a perturbation analysis a similar trend was also observed, namely the residual liquid film thicknesses for various values of the power-law index are almost identical at low capillary numbers.

References

[1] G.I. Taylor, J. Fluid Mech. 10 (1961) 161.
[2] F.P. Bretherton, J. Fluid Mech. 10 (1961) 166.
[3] C.W. Park, G.M. Homsy, J. Fluid Mech. 139 (1984) 291.
[4] T.S. Ro, G.M. Homsy, J. Non-Newtonian Fluid Mech. 57 (1995) 203.
[5] B.G. Cox, J. Fluid Mech. 14 (1962) 81.
[6] B.G. Cox, J. Fluid Mech. 20 (1964) 193.
[7] D.A. Reinelt, Phys. Fluids 30 (1987) 2617.
[8] F. Kamisli, Mathematical Analysis and Experimental Study of Gas-Assisted Injection Molding, Ph. D. Dissertation, State University of New York at Buffalo, 1997.
[9] P.C. Huzyak, K.W. Koelling, J. Non-Newtonian Fluid Mech. 71 (1997) 73.
[10] J. Ratulowski, H.C. Chan, Phys. Fluids A 1 (1989) 1642.
[11] W.B. Kolb, R.L. Cerro, Phys. Fluids A 5 (1993) 1549.
[12] D.A. Reinelt, J. Fluid Mech. 183 (1987) 219.
[13] J.A. Tallmadge, Chem. Eng. Sci. 24 (1969) 471.
[14] J.A. Tallmadge, AIChE 16 (1970) 925.
[15] R.P. Spiers, C.V. Subbaraman, W.L. Wilkinson, Chem. Eng. Sci. 30 (1975) 379.
[16] L.D. Landau, V.G. Levich, Acta Physicochim URSS 17 (1942) 42.
[17] W.B. Kolb, R.L. Cerro, Chem. Eng. Sci. 46 (1991) 2181.
[18] M. Van Dyke, Perturbation Methods in Fluid Mechanics, Parabolic Press, CA, 1975.
[19] A.H. Nayfeh, Perturbation Methods, Wiley, New York, 1973.
[20] F. Fairbrother, A.E. Stubbs, J. Chem. Soc. 1 (1935) 527.
[21] J.M. McLean, P.G. Saffman, J. Fluid Mech. 102 (1981) 455.
[22] R.H. Marchessault, S.G. Mason, Ind. Eng. Chem. 52 (1960) 79.
[23] E. Pitts, J. Fluid Mech. 97 (1980) 53.
[24] L.W. Schwart, H.W. Princen, A.D. Kiss, J. Fluid Mech. 172 (1986) 259.
[25] P. Tabeling, G. Zocchi, A. Libchaber, J. Fluid Mech. 177 (1987) 67.
[26] P.G. Saffman, G.I. Taylor, Proc. R. Soc. Lond. A 245 (1958) 312.